Available online at www.sciencedirect.com
SCIENCE DIRECT
Journal of Power Sources 156 (2006) 71–77
JOURNAL OF POWER SOURCES
www.elsevier.com/locate/jpowsour

# Identification of a nonlinear model for the electrical behavior of a solid oxide fuel cell

Markus Haschka [a,*], Thomas Weickert [a], Volker Krebs, Sven Schäfer [b], Ellen Ivers-Tiffée [b]

[a] *Institut für Regelungs- und Steuerungssysteme, Universität Karlsruhe (TH), Karlsruhe 76131, Germany*
[b] *Institut für Werkstoffe der Elektrotechnik, Universität Karlsruhe (TH), Karlsruhe 76131, Germany*

Available online 20 October 2005

**Abstract**

In this contribution, a dynamical nonlinear model structure for the identification of the electrical behavior of a solid oxide fuel cell is developed using expert knowledge from material scientists. The estimation of the model parameters can be realized by an iterative algorithm based on analytical equations to determine parameter estimates in each iteration step. An enhancement of the estimation can be achieved by an additional numerical optimization of the model parameters. Furthermore, this model can be extended to represent the time dependency of the model due to deterioration of the fuel cell materials.


*Keywords:* Solid oxide fuel cell; System identification; Degradation of materials

## 1. Introduction

For many purposes a mathematical model of a solid oxide fuel cell (SOFC) is required. For instance, this model allows to separate the formation effects from the usual current/voltage-dynamics during the first startup procedure of a SOFC [1]. During operation, it could be used to develop a control strategy for load changes. And finally, a dynamical model can represent the effects of deterioration of a SOFC-system. Recent publications like [2–4]. address the modeling of these systems. In [2] and [4] a physical approach was used to represent the dynamic behavior of the fuel cell. To obtain a lower order linear model of the SOFC-dynamics an identification procedure was proposed in [3]. The paper is organized as follows: in Section 2, an appropriate model structure will be developed. Afterwards, an identification for a time-invariant parametric model is proposed in Section 3. In order to improve the mathematical representation, a time-variant model will be estimated in Section 4. Finally, in Section 5 a simple approach to represent degradation effects is given.

## 2. Development of a model structure

In this paragraph a model structure for the current-density/voltage-loss-behavior will be developed. The cathode material of the considered SOFC is (La,Sr)$MnO_{3-}$ which is abbreviated as LSM. Yttrium doped Zirconia 8YSZ (8 mol% $Y_2O_3$ doped $Zr0_2$) is the electrolyte material. Finally, the anode consists of a Ni/8YSZ-cermet.

In Fig. 1, measurement data of a SOFC are given. Based on the same measurement, the corresponding voltage-loss versus current-density is depicted in Fig. 2. The latter plot shows that the electrical behavior is dominated by a static transfer element and that dynamic effects are less significant. This suggests the following modeling approach

$$u(kT) = u_N(kT) + u_H(kT), \tag{1}$$

$$u_N(kT) = N(j_c(kT)), \tag{2}$$

$$u_H(kT) = \mathcal{Z}^{-1}\left\{L(z^{-1})\right\} * \phi(j_c(kT)), \tag{3}$$

where $u(kT)$ is the voltage loss and $j_c(kT)$ denominates the current density of the fuel cell, $T$ is the constant sampling time and $k$ is the index for the sampled measurement data. In (1), the voltage loss is the sum of a nonlinear function $N(j_c)$ of the current density $j_c$ and the response of a Hammerstein-model [5] consisting of a linear system $L(z^{-1})$ whose input signal is a function $\phi(j_c)$ of the

* Corresponding author.
*E-mail addresses:* haschka@irs.uni-karlsruhe.de (M. Haschka), krebs@irs.uni-karlsruhe.de (V. Krebs), sven.schaefer@iwe.uni-karlsruhe.de (S. Schäfer), ellen.ivers@iwe.uni-karlsruhe.de (E. Ivers-Tiffée).

0378-7753/$ – see front matter © 2005 Elsevier B.V. All rights reserved.
doi:10.1016/j.jpowsour.2005.08.014

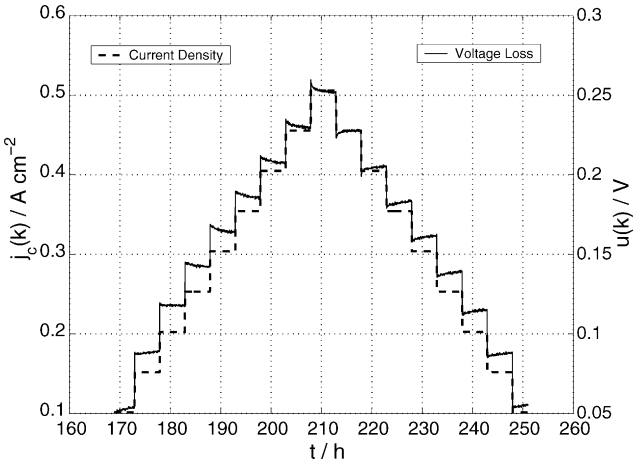


Fig. 1. Current-density/voltage-loss-measurements vs. time.

current density $j_c$. The symbol "$*$" in (3) indicates the convolution operator. The current-density/voltage-loss-measurement in Fig. 2 is mainly represented by the function $N(j_c)$. Some assumptions have to be made in order to specify the model structure (1)–(3) in more detail. It is known that two reversible processes in the materials are responsible for the dynamic behavior of the SOFC which will be represented by the linear system $L(z^{-1})$ and the unknown function $\phi(j_c)$:

(1) Temperature effect: a changing current density causes a temperature change of the material which results in a decrease or an increase of conductivity. The time constant of this process is about 3–5 min.
(2) Structural effect: a changing current density causes a change of the local oxygen partial pressure at the cathode/electrolyte interface. The oxygen partial pressure has an impact on the oxygen vacancy concentration in the cathode grain [6]. Therefore, the size of the electrochemical active triple phase boundary at the cathode/eletrolyte interface is affected. In Fig. 3, the triple phase boundary at the cathode–electrolyte interface in equilibrium is depicted schematically. An instantaneous current density step causes an increase of the area specific current density at the triple phase boundary. This effect is shown in Fig. 4. The size of the triple phase boundary increases due to the higher area specific current density. This effect could be explained by a depletion of oxygen in the cathode grain. After 1–5 h, the triple phase boundary is in the equilibrium state for the new higher current density (Fig. 5). Thus, the conductivity is increased by the increase of the triple phase boundary.

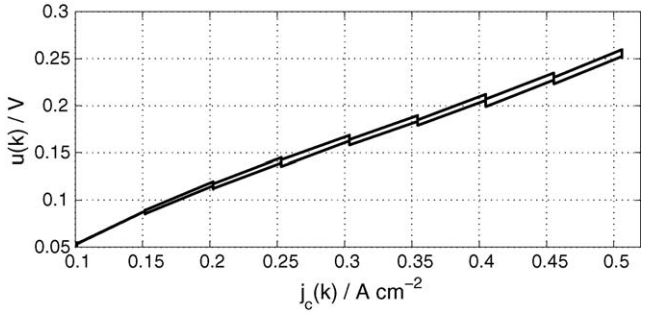


Fig. 2. Current-density vs. voltage-loss.

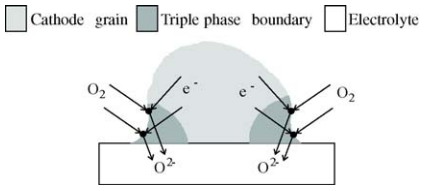


Fig. 3. TPB in equilibrium before a current density change.

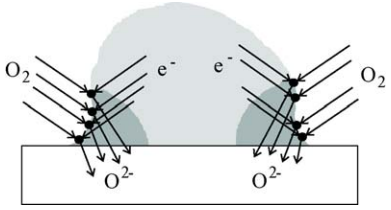


Fig. 4. TPB immediately after an increase of the current density.

The model order of the linear system $L(z^{-1})$ is chosen as $n_L = 2$, in order to represent the two considered dynamical effects, leading to the transfer function

$$L(z^{-1}) = \frac{b_0 + b_1 z^{-1} + b_2 z^{-2}}{1 + a_1 z^{-1} + a_2 z^{-2}}.$$

In order to separate the stationary behavior and the dynamical behavior, the linear systems output signal has to vanish for constant input signals. For constant input signals $j_c$, the output signal is solely determined by the nonlinear function $N(j_c)$. This leads to a constraint for the numerator of the linear system. To meet this condition, the linear system $L(z^{-1})$ has to have a differentiating behavior. Time discrete systems with a zero at $z = 1$ show this property. The constraint

$$b_0 + b_1 + b_2 = 0 \tag{4}$$

for the model parameters $b_0$, $b_1$ and $b_2$ guarantees that the linear systems response equals zero in steady-state.

It is also known that the time constants of the two processes depend on the sign of $\mathrm{d}j_c/\mathrm{d}t = \dot{j}_c$. Therefore, the estimation of two different linear systems is necessary, one system for increasing current densities and a different one for decreasing current densities. For $\dot{j}_c \geq 0$ the linear model $L(z^{-1})$ is denoted as $L_{\mathrm{up}}(z^{-1})$ and for $\dot{j}_c < 0$ it is denoted as $L_{\mathrm{down}}(z^{-1})$.

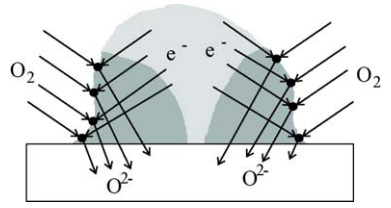


Fig. 5. TPB in equilibrium after the current increase.

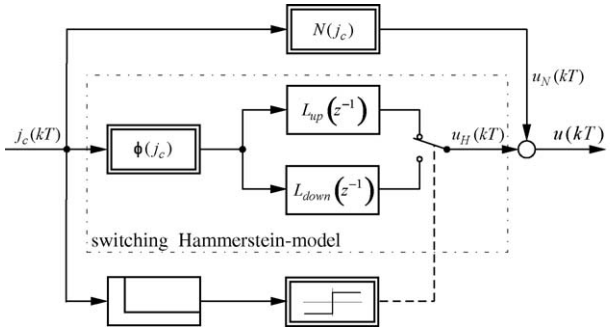


Fig. 6. Structure of the identification model in most cases.

For the nonlinearity $N(j_c)$, a polynomial approach

$$N(j_c) = c_0 + c_1 j_c + c_2 j_c^2 + \cdots + c_{n_N} j_c^{n_N} \tag{5}$$

is proposed. The degree $n_N = 3$ for the polynomial $N(j_c)$ in (5) is adequate in most cases.

This model structure is depicted in Fig. 6. In the sequel, the unknown model parameters of this model structure will be determined from measurement data.

## 3. Iterative identification of the model parameters of the time-invariant model

In this section, a parameter identification algorithm for the time-invariant model structure in Fig. 6 is presented. By analysis of measurement results, it turns out that the unknown function $\phi(j_c)$ could be chosen as $\phi(j_c) = j_c^2$. Therefore, the model parameters of the time-invariant model structure in Fig. 6 are

$$\underline{\theta}_{TI} = [c_0, c_1, c_2, c_3; a_{1,up}, a_{2,up}; a_{1,down}, a_{2,down}; b_{0,up}, b_{1,up}, b_{2,up}; b_{0,down}, b_{1,down}, b_{2,down}]. \tag{6}$$

The indices "up" and "down" of some model parameters in (6) denote their affiliation to the linear submodels $L_{up}(z^{-1})$ or $L_{down}(z^{-1})$.

The basic approach in parameter identification is to formulate the identification problem as an optimization problem. Most commonly, a quadratic performance index

$$J_{TI}(\underline{\theta}_{TI}) = \sum_{k=1}^{N} \left(y_{meas}(k) - y_{model}(\underline{\theta}_{TI}, k)\right)^2 \tag{7}$$

is defined, where $y_{meas}(k)$ are measured, noisy data from the output of the process and $y_{model}(\underline{\theta}_{TI}, k)$ are the simulated output data from the used identification model (Fig. 6) with the parameter vector $\underline{\theta}_{TI}$. A numerical optimization algorithm could minimize the function (7) under the constraint (4). With sufficient initial values for this optimization, the determination of the global minima of the function $J_{TI}(\underline{\theta}_{TI})$ is more likely. The determination of these initial values is given by an iterative algorithm using the dominating influence of the static element $N(j_c)$ on the transfer behavior. The steps of this algorithm are depicted in the function chart in Fig. 7:

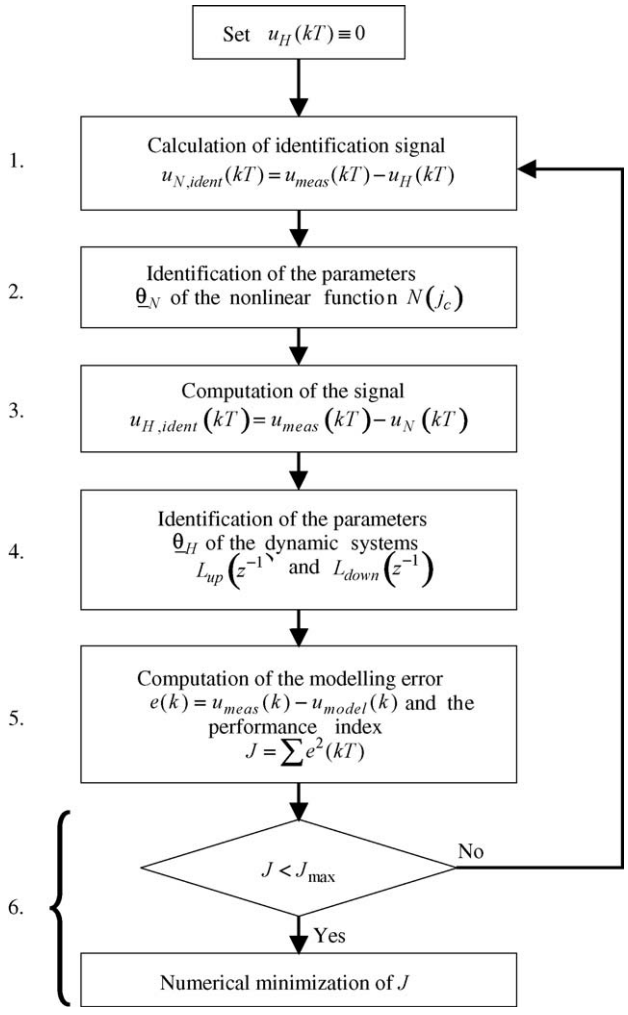


Fig. 7. Function chart of the identification algorithm.

(1) The difference signal $u_{N,ident} = u_{meas}(kT) - u_H(kT)$ is calculated using the up to date Hammerstein-Model $u_H(kT)$. In the first initialization, this signal is set to $u_H(kT) = 0$, to neglect the influence of the small signal $u_H(kT)$ on the absolute value $u(k)$ (see Fig. 2).
(2) The model parameters $\underline{\theta}_N$ of the polynomial $N(j_c)$ are estimated by the least-squares-algorithm [5,7] using $u_{N,ident}$ which was computed in step 1.
(3) With the model parameters $\underline{\theta}_N$ it is possible to separate the signals $u_H(kT)$ and $u_N(kT)$ in the measurement data $u_{meas}(kT)$. The signal $u_{H,ident}(kT) = u_{meas}(kT) - u_N(kT)$ is computed.
(4) Using $u_{H,ident}(kT)$, the linear subsystems $L_{up}(z^{-1})$ and $L_{down}(z^{-1})$ will be estimated taking constraint (4) into account. This estimation is computed with Eq. (A.5), derived in Appendix A.
(5) Using all currently estimated parameters gives the modeling error of the model parameter set $J(\underline{\theta}_{TI}) = \Sigma e^2(k)$.
(6) If $J(\underline{\theta}_{TI}) < J_{max}$ is not fulfilled, the algorithm jumps to step 1 using the estimated signal $u_H(kT)$.

If $J(\underline{\theta}_{TI}) < J_{max}$, a numerical minimization of $J(\underline{\theta}_{TI})$ with respect to the model parameters $\underline{\theta}_{TI}$ gives the improved esti-

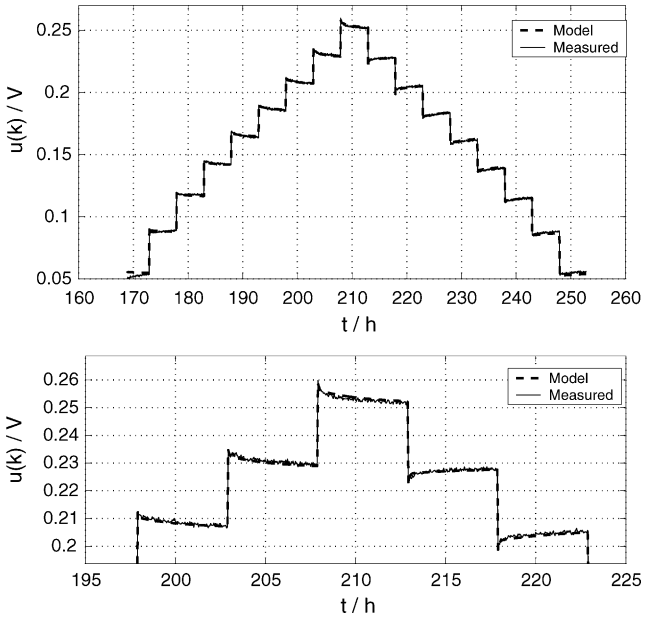


Fig. 8. Voltage loss of the model and measurement data.

mated value for $\hat{\underline{\theta}}_{\mathrm{TI}}$. This minimization is necessary because it is not guaranteed that the iterative execution of steps 1–5 yields the global minimum of $J(\underline{\theta}_{\mathrm{TI}})$.

The result of an estimation using the measurement data from Fig. 1 is shown in Fig. 8. This plot shows that the model structure (1)–(3) is an appropriate modeling approach, because the modeling error is very small. In Appendix B, a transformation is given to separate the two dynamical processes. With (B.7), the time constants of the two processes can be determined, which makes the allocation of the two processes possible. For this identification result, the time constants are:

$$\begin{aligned} \tau_{1,\mathrm{up}} &= 3.52\ \mathrm{min} \quad \tau_{1,\mathrm{down}} = 4.08\ \mathrm{min} \\ \tau_{2,\mathrm{up}} &= 2.47\,\mathrm{h} \quad \tau_{2,\mathrm{down}} = 4.9\,\mathrm{h} \end{aligned} \tag{8}$$

The values for the time constants in (8) indicate that process 1 is the temperature effect and process 2 is the structural effect. In Fig. 9, the voltage losses of these two processes are shown for a section of the measurement period. The term $u_{\mathrm{TE}}$ designates the temperature effect voltage and $u_{\mathrm{SE}}$ designates the voltage of the structural effect. The plot shows that the voltage-loss of the structural effect is by far more significant for the dynamical behavior. An additional advantage of the identification procedure proposed in this paper is that the current-density/voltage-loss characteristic could be estimated simultaneously to the estimation of the SOFC-dynamics. The estimated current-density/voltage-loss characteristic is shown in Fig. 10.

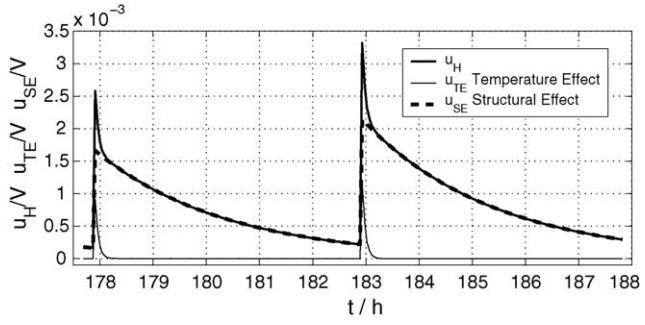


Fig. 9. Separation of the two dynamical effects.

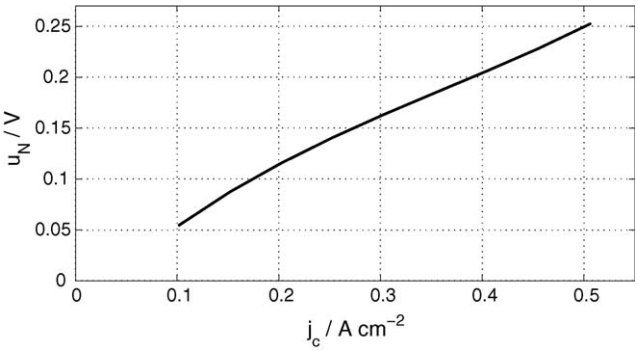


Fig. 10. Identified current-density/voltage-loss-characteristic $N(j_c)$.

The proposed identification method was also applied successfully on other measurement data taken from solid oxide fuel cells, resulting to different values for the model parameters than those determined in this paper.

## 4. Time-variant model identification

Until now, a time-invariant parametric model was identified. However, it is known that the electrical behavior of SOFC-systems changes during large time-periods. Fig. 11 demonstrates the time variance of the considered fuel cell. The continuous line is the current-density/voltage-loss measurement which was used for the identification of the voltage loss model in Section 3. The measurement data between 410 and 490 h is depicted as a dotted line in the same figure. Clearly, it can be recognized by analyzing this plot that the current-density/voltage-loss characteristic could not be assumed as time-invariant. The linear component of the characteristic $c_1$ has changed most significant during operation of the fuel cell. Therefore, a time-variant model for the voltage loss will be estimated in this section in order to improve the representation of the real physical behavior.

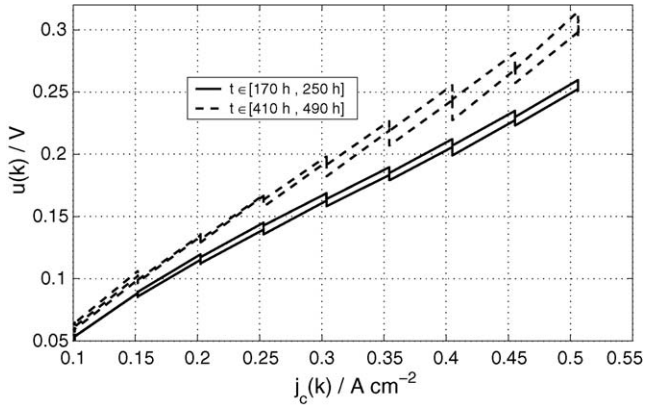


Fig. 11. Measurements of current-density vs. voltage-loss.

A simple but common method used in the field of identification is the minimization of an exponentially weighted sum

$$J_{\mathrm{TV}}(\underline{\theta}_{\mathrm{TV}}, i) = \sum_{k=0}^{i} \underbrace{\mathrm{e}^{-\beta(i-k)}}_{w_\beta(k)} (y_{\mathrm{meas}}(k) - y_{\mathrm{model}}(\underline{\theta}_{\mathrm{TV}}(i), k))^2 \quad (9)$$

of the modeling error. The weighting factor has to weight the present output error stronger than the errors from the past [8]. The forgetting factor $\beta > 0$ has to be chosen suitable to detect variations of the model parameters. On the other hand, the forgetting factor should not be too large in order to keep the influence of the measurement noise on the identification result limited. For each index value $i$ a numerical minimization of the weighted performance index (9) gives a snapshot of the system behavior at the time $iT$, because the vector $\underline{\theta}_{\mathrm{TI}}(i)$ of the model parameters is also time-variant. The numerical minimization uses the previous estimated time-variant parameter-vector $\underline{\hat{\theta}}_{\mathrm{TI}}(i-1)$ as the initial value for the estimation of the current estimation of $\underline{\hat{\theta}}_{\mathrm{TI}}(i)$, because the changes between two time instants can be assumed as very small. The first identification uses the time-invariant parameters $\underline{\hat{\theta}}_{\mathrm{TI}}$ as initial values.In advance of the execution of the time-variant identification, it is necessary to decide which model parameters will be time variant. A high degree of freedom causes a very good identification accuracy, but it will not be possible to interpret the result. Therefore, the degree of freedom has to be reduced. As already mentioned, Fig. 11 demonstrates that the parameter $c_1$, which represents the ohmic component of the characteristic, changes most significantly. Therefore, it will be sufficient to assume that only $c_1$ varies with respect to time. All other model parameters will be assumed as time-invariant. The result of the numerical optimization for the identification of the time-variant $c_1(i)$ is shown in Fig. 12. The identification algorithm for the parameter $\underline{\hat{\theta}}_{\mathrm{TI}}$ starts at $i = 5690$. Fig. 12 shows that the parameter $c_1$ increases monotonically, if the voltage loss is increasing. A constant or a decreasing voltage-loss has a very faint influence on the change of $c_1$. This result is surprising, because it shows that an increase of voltage-loss has a more significant influence on the degradation of the SOFC than constant high current densities.

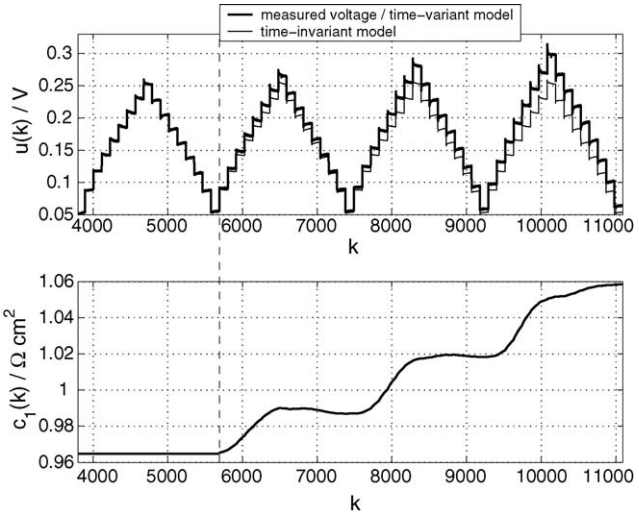


Fig. 12. Identification of the time-variant parameter $c_1(k)$.

This surprising new result can be explained by the structural effect. In Figs. 3–5, this effect is sketched schematically for a current density increase. It takes 1–5 h to get in the equilibrium state. During this time period the triple-phase-boundary increases and causes a decrease of the voltage-loss. During the settling time, the voltage loss and the area specific current density at the triple-phase-boundary is very high. Area specific current densities have a strong influence on the materials at the triple phase boundary. In [1], the area specific current density causes a decrease of losses during the formation of the cathode/electrolyte-interface of SOFCs. Here, the locally high loss during the settling time after an increase of current density causes degradation of the SOFC (increase of the ohmic losses), the efficiency of the cell diminishes. This observed degradation process will be modeled in the next section.

## 5. Model for the degradation effects

In order to predict the status of the fuel cell materials, the observed degradation effect has to be represented by a mathematical model. As demonstrated in Fig. 12, an increase of the current density causes an increase of the model parameter $c_1$, which represents the ohmic resistance in the current-density/voltage-loss-characteristic $N(j_c)$. A possible explanation for this increase is a locally concentrated high current density at the triple-phase-boundary at the cathode/electrolyte-interface. A possible mathematical approach is the use of the voltage loss of the structural effect $u_{\mathrm{SE}}$ as an input signal of a discrete-time integrator. To take into account that $c_1$ does not increase for decreasing current densities, only positive values of $u_{\mathrm{SE}}$ should have an impact on the degradation in the model. The result is the model

$$\begin{aligned} c_1(k) &= c_1(k-1) + T\delta(u_{\mathrm{SE}}^{+}(kT)) \\ &= c_1(k-1) + T[d_0 + d_1 u_{\mathrm{SE}}^{+}(kT)) + d_2(u_{\mathrm{SE}}^{+}(kT))^2 \\ &\quad + d_3(u_{\mathrm{SE}}^{+}(kT))^3 + d_4(u_{\mathrm{SE}}^{+}(kT))^4], \end{aligned} \quad (10)$$

which is used to represent the degradation (the increase of $c_1$), with

$$u_{\mathrm{SE}}^{+} = \begin{cases} u_{\mathrm{SE}} & \text{for} \quad u_{\mathrm{SE}} \geq 0 \\ 0 & \text{for} \quad u_{\mathrm{SE}} < 0 \end{cases}$$

as the input signal. $T\,\delta(u_{\mathrm{SE}}^{+}(kT))$ is the difference $c_1(k) - c_1(k-1)$, hence the $\delta$ value could be interpreted as the velocity of the degradation. The determination of the model parameters

$$\underline{\theta}_{\mathrm{deg}} = [d_0\, d_1\, d_2\, d_3\, d_4]$$

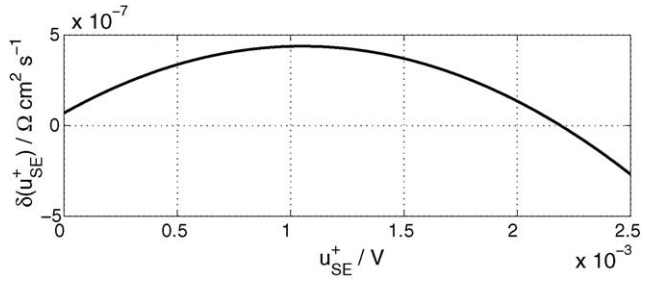


Fig. 13. Voltage $u_{SE}^{+}$ and time-dependent parameter $c_1$.

of the degradation model (10) is done by a numerical minimization of the performance index

$$J_{\text{deg}}(\underline{\theta}_{\text{deg}}) = \sum_{k=1}^{N} (y_{\text{meas}}(k) - y_{\text{model}}(\underline{\theta}_{\text{deg}}, k))^2$$

for the output error $y_{\text{meas}}(k) - y_{\text{model}}$ of the voltage loss model, where $c_1(k)$ is time-variant and given by (10). The other model parameters are the time-invariant estimates from Section 3. In Fig. 13, the estimated function $\delta(u_{SE}^{+})$ is shown for the measurement data. The interception point of the plot with the $\delta$-axis gives the increase of $c_1$ for the steady state operation ($u_H = u_{SE}^{+} = 0$). For $0 < u_{SE}^{+} < 1$ mV the degradation velocity $\delta(u_{SE}^{+}(kT))$ is increasing monotonically. For high values $u_{SE}^{+} < 1$ mV, $\delta$ is decreasing. In [1], it was demonstrated how high area specific currents could improve the cell performance during the formation process. Thus, a possible physical explanation for the smaller degradation velocity $\delta$ is that the formation of the cathode/electrolyte-interface is continued, due to very high area specific current densities for $u_{SE}^{+} < 1$ mV.

## 6. Conclusions and outlook

A useful model structure for the current-density/voltage-loss dynamic for a single SOFC is developed. The model structure of the generally nonlinear model consists of a static element for the steady-state equilibrium characteristic and a switching Hammerstein-Modell for transitions between different equilibrium states. A simple and fast identification algorithm is developed to identify the model parameters of this time invariant model. However, for long term simulations of the voltage-loss of a fuel cell, the identified time invariant model is not suitable. This can be explained by changes in the cathode/electrolyte-interface caused by a locally high area specific current density. In order to represent the time dependency, a time-variant model is identified using an exponentially weighted performance index. A numerical optimization gives the estimated value for a significant time dependent parameter. Using the time dependency of the voltage-loss model, a simple approach is given to represent the coherence leading to the fuel cell degradation during fast changes of the current density. A low order nonlinear degradation model is estimated by a numerical optimization algorithm. This model can be used to develop control strategies for a safe operation of SOFC-systems in order to allow a long durability, because the expected degradation of the fuel cell materials can be predicted by this model.

## Acknowledgment

This work was supported by the Deutsche Forschungsgemeinschaft (DFG) under contracts no. Kr 949/12-1 and Iv 14/6-1.

## Appendix A. Least-squares-estimation with a linear constraint

Given is the performance index function

$$J(\underline{\theta}) = (\underline{y} - \underline{M\theta})^T (\underline{y} - \underline{M\theta}) \tag{A.1}$$

and the linear equation

$$\underline{N\theta} = \underline{b}. \tag{A.2}$$

Objective is finding a $\hat{\underline{\theta}}$ which minimizes the function (A.1) and meets the constraint (A.2). This problem will be solved by using the method of the Lagrangian multipliers. The new function

$$L(\underline{\theta}) = J(\underline{\theta}) + \underline{\lambda}^T (\underline{N\theta} - \underline{b})$$

is defined, whose derivation with respect to the variable $\underline{\theta}$ and the Lagrangian multiplier $\underline{\lambda}$ gives the necessary conditions

$$\left.\frac{\partial L(\underline{\theta})}{\partial \underline{\theta}}\right|_{\underline{\theta}=\hat{\underline{\theta}}} = -2\underline{M}^T \underline{y} + 2\underline{M}^T \underline{M}\hat{\underline{\theta}} + \underline{N}^T \underline{\lambda} = 0, \tag{A.3}$$

$$\left.\frac{\partial L(\underline{\theta})}{\partial \underline{\lambda}}\right|_{\underline{\theta}=\hat{\underline{\theta}}} = \underline{N\hat{\theta}} - \underline{b} = 0 \tag{A.4}$$

to solve this optimization problem. Using the conditions (A.3) and (A.4) gives the solution

$$\hat{\underline{\theta}} = \underline{PM}^T \underline{y} + \underline{PN}^T \underline{Q}(\underline{b} - \underline{NPM}^T \underline{y}) \tag{A.5}$$

if the matrices

$$\underline{P} = (\underline{M}^T \underline{M})^{-1} \quad \text{and} \quad \underline{Q} = (\underline{N}^T \underline{M})^{-1} \underline{N}^T)^{-1}$$

exists.

## Appendix B. Separation of the dynamic effects

The transfer function of the linear system

$$L(z^{-1}) = \frac{b_0 + b_1 z^{-1} + b_2 z^{-2}}{1 + a_1 z - 1 + a_2 z^{-2}}, \quad b_0 + b_1 + b_2 = 0 \tag{B.1}$$

has to be transformed on the form

$$L(z^{-1}) = \underbrace{k_1 \frac{1 - z^{-1}}{1 - p_1 z^{-1}}}_{L_1(z^{-1})} + \underbrace{k_2 \frac{1 - z^{-1}}{1 - p_2 z^{-1}}}_{L_2(z^{-1})} \tag{B.2}$$

where the two dynamic effects $L_1(z^{-1})$ and $L_2(z^{-1})$ can be investigated separately. The representation of (B.2) is not unique,

because two solutions are possible due to the permutability of the parameters. Thus, one possible solution is

$$k_1 = b_0 + \frac{b_2 - b_0\left((-a_1/2) + \sqrt{(a_1^2/4) - a_2}\right)}{-(a_1/2) + \sqrt{(a_1^2/4) - a_2} - (a_2)/\left(-(a_1/2) + \sqrt{(a_1^2/4) - a_2}\right)}, \tag{B.3}$$

$$k_2 = \frac{b_0\left(-(a_1/2) + \sqrt{(a_1^2/4) - a_2}\right) - b_2}{-(a_1/2) + \sqrt{(a_1^2/4) - a_2} - \left(a_2/\left(-(a_1/2) + \sqrt{(a_1^2/4) - a_2}\right)\right)}, \tag{B.4}$$

$$p_1 = \frac{a_2}{-(a_1/2) + \sqrt{(a_1^2/4) - a_2}}, \tag{B.5}$$

$$p_2 = -\frac{a_1}{2} + \sqrt{\frac{a_1^2}{4} - a_2}. \tag{B.6}$$

The time constants of the two processes are

$$\tau_i = -\frac{T}{\ln p_i}, \quad 0 < p_i < 1, \quad p_i \in \mathbb{R} \quad i \in \{1, 2\}. \tag{B.7}$$

## References


[1] S. Schäfer, A. Krügel, A. Weber, E. Ivers-Tiffée, Cathode Polarization Resistance: A Modeling Approach, European Solid Oxide Fuel Cell Forum 2004, Lucerne, Switzerland, Vol. 129, pp. 205–215, 2004.

[2] J. Padullés, G. Ault, J. McDonald, An integrated SOFC plant dynamic model for power systems simulation, J. Power Sources 86 (2000) 495–500.

[3] F. Jurado, Modeling SOFC plants on the distribution system using identification algorithms, J. Power Sources 129 (2004) 205–215.

[4] O. Tomoyuki, M. Koyama, C.-J. Wen, K. Yamada, H. Takahashi, Object-based modeling of SOFC system: Dynamic behavior of micro-tube SOFC, J. Power Sources 129 (2004) 205–215.

[5] L. Ljung, System Identification-Theory for the User, P.T.R. Prentice Hall, Englewood Cliffs, NJ, 1987.

[6] A. Hammouche, E. Siebert, A. Hammou, M. Kleitz, A. Caneiro, Electroanalytic properties and nonstoichiometry of the temperature air electrode $La_{(1-x)}Sr_xMnO_3$, J. Power Sources 129 (2004) 205–215.

[7] G.C. Goodwin, R.L. Payne, Dynamic System Identification: Experiment Design and Data Analysis, Academic Press, New York, 1987.

[8] P. Young, Recursive Estimation and Time-Series Analysis, Springer-Verlag, 1984.